

ARTICLE OPEN



Comprehensive behavioral characterization and impaired hippocampal synaptic transmission in R1117X Shank3 mutant mice

Jingyao Gao^{1,4}, Shumin Wu^{1,4}, Jingxuan Yang¹, Tong Ye¹, Jie Yang¹, Wenhua Shen¹, Xingwang Chen¹, Li Huang¹, Ruiqi Pang², Ping Lin¹, Jiahe Lin^{1,3}, Yi Zhou², Wei Wang¹ and Tao Tan¹✉

© The Author(s) 2025

Mutations in the *Shank3* gene are strongly associated with various neurodevelopmental disorders, particularly autism spectrum disorder (ASD). The R1117X mutation, which results in truncated SHANK3 protein, has been implicated in dysfunctions in the striatum and cortex. However, its effects on hippocampal function remain poorly understood. In this study, we performed a comprehensive behavioral and synaptic analysis of homozygous R1117X Shank3 mutant mice. These mice exhibited deficits in sensory gating, motor coordination, and pain perception, alongside severe anxiety in novel environment. Additionally, they showed significant impairments in learning and memory, as well as abnormal spontaneous fine motor behaviors. Histological analysis revealed morphological changes in the hippocampus, which were coupled with deficits in synaptic transmission and plasticity. Notably, we observed a downregulation of glutamatergic receptors in the hippocampus, particularly NMDA receptor subtypes. Taken together, these findings demonstrate that the homozygous R1117X Shank3 mutant mouse represents a valuable model for investigating schizophrenia associated with intellectual disability. The altered hippocampal morphology, impaired synaptic function, and deficits in learning and memory observed in this model provide new insights into the underlying mechanisms of *Shank3*-related neurodevelopmental disorders.

Translational Psychiatry (2025)15:274; <https://doi.org/10.1038/s41398-025-03505-1>

BACKGROUND

Autism spectrum disorder (ASD) is a neurodevelopmental condition characterized by high heritability and deficits in social communication and interaction, along with repetitive behaviors [1]. The etiology of ASD is strongly linked to genetic factors, involving complex interactions between common and rare genetic variants affecting numerous genes [2]. To investigate the mechanisms and potential treatments for ASD, researchers have employed various transgenic mouse models. These models have been created by targeting high-risk genes via knockout, knock-in, and mutation techniques [1]. Notable models include transgenic mice related to *Shank3* [3], *CNTNAP2* [4], *CHD8* [5], and 16p11 duplication/deletion [6].

Truncating mutations in the *SHANK* gene family (*SHANK1*, *SHANK2*, and *SHANK3*) account for approximately 1% of all ASD cases [7], a surprisingly high percentage given the etiological diversity of ASD. Among these genes, *SHANK3* (Src homology 3 (SH3) and multiple ankyrin repeat domains 3) is recognized as a significant monogenic cause of ASD [8]. The *SHANK3* (human) or *Shank3* (rodent) gene is located on chromosome 22q13.3 in humans (<https://www.ncbi.nlm.nih.gov/gene/85358>) and on chromosome 15E3 in mice (<https://www.ncbi.nlm.nih.gov/gene/58234>).

It comprises 22 exons and encodes the SHANK3 protein, which includes various functional domains, such as an N-terminal ankyrin repeat domain, an SH3 domain, a PSD-95/discs large/zonula occludens-1 (PDZ) domain, several proline-rich regions, and a C-terminal sterile α -motif (SAM) domain (Figure S1A) [9]. SHANK3 serves as a scaffold protein in the postsynaptic density (PSD) of glutamatergic synapses, interacting with key synaptic components essential for synaptic organization and function [10].

Patients with 22q13.3 deletion are diagnosed with Phelan McDermid Syndrome (PMDS) [11], an ASD characterized by hypotonia, impaired language skills, and intellectual disability (ID). Studies in human genetics [12] and animal models [13] have highlighted the role of *Shank3* haploinsufficiency, resulting from deletion or spontaneous mutation, in the development of ASD [14]. Various strategies targeting *Shank3* to mimic PMDS pathologies have been developed in rodent models [15], including constitutive knockout (KO) models that affect different exons and promoters, conditional KO models (cKOs) with cell type-specific *SHANK3* deficiency, and knock-in (KI) strategies incorporating mutations identified in ASD patients.

Multiple point/misense mutations at different exons or functional domains of *SHANK3* have been generated based on

¹Oujiang Laboratory (Zhejiang Lab for Regenerative Medicine, Vision and Brain Health), Institute of Aging, Key Laboratory of Alzheimer's Disease of Zhejiang Province, Zhejiang Provincial Clinical Research Center for Mental Disorders, The Affiliated Wenzhou Kangning Hospital, Wenzhou Medical University, Wenzhou, Zhejiang 325000, P. R. China.

²Department of Neurobiology, Army Medical University, Chongqing 400038, China. ³Department of Neurology, Tongji Hospital, Tongji Medical College, Huazhong University of Science and Technology, Wuhan, Hubei 430000, P. R. China. ⁴These authors contributed equally: Jingyao Gao, Shumin Wu. ✉email: tantao@ojlab.ac.cn

Received: 1 December 2024 Revised: 18 June 2025 Accepted: 30 July 2025

Published online: 09 August 2025

clinical cases [15]. While targeting the proline-rich regions of exon 21, ASD-related mutations, including InsG3728 [16] and InsG3680, and the schizophrenia-associated mutation R1117X [17] have been generated. All these mutations result in truncated SHANK3 proteins.

The nonsense R1117X mutation has been previously linked to striatal and cortical dysfunctions [17]. However, since the R1117X mutation has been found in patients with schizophrenia and is associated with mental retardation [18], the cognition-related behavioral phenotypes require further exploration. Additionally, mechanisms in other cognition-related brain regions, especially the hippocampus, warrant in-depth investigation. In this study, we explored the detailed behavioral characteristics and neural mechanisms within the hippocampus of R1117X mice, providing new evidence for understanding different mutations of the *Shank3* gene in ASD.

METHOD

Animals

C57BL/6J background R1117X *Shank3* (*Shank3**R1117X KI) mice were purchased from the Shanghai Model Organisms Center (NMX-KI-192008). The R1117X *Shank3* knock-in allele harbors the schizophrenia-associated R1117X nonsense mutation in *Shank3* exon 21 on chromosome 15, resulting in the expression of a ~122 kDa truncated SHANK3 protein [17]. All experiments utilized age-matched homozygous R1117X *Shank3* (*Shank3*) or wild-type (WT) male mice, which were between 8 and 12 weeks of age. The animals were housed in groups under a 12-h light/dark cycle and were provided with food and water *ad libitum*. All animal care and experimental procedures were approved by the Institutional Animal Care and Use Committee of Oujiang Laboratory.

Genotyping

Mouse tails (approximately 0.1 cm) were collected and placed into 1.5 mL Eppendorf tubes separately. Each tube was filled with 0.5 mL of lysis buffer (AG21010, Accurate Biology) and 50 μ L of protease K solution (AG12004, Accurate Biology). The tubes were incubated overnight at 56°C. The samples were centrifuged at 12,000 rpm for 10 min at room temperature. The supernatant was transferred to 1.5 mL Eppendorf tubes, and 1 mL of ethanol (approximately twice the volume of the supernatant) was added. The tubes were gently shaken to induce flocculent precipitation and then centrifuged at 13,000 rpm for 15 min. The supernatant was discarded, and the pellet was washed with 1 mL of 70% ethanol, followed by another centrifugation at 13,000 rpm for 10–15 min. The supernatant was discarded, and the pellet was air-dried at room temperature for 15 min. Finally, 80–100 μ L of sterilized water was added to each tube, and the samples were allowed to dissolve completely at room temperature or 37°C for 1 h. Polymerase chain reaction (PCR) was performed once the DNA was fully dissolved [17]. The primers used for the identified genotypes are listed in Table 1.

Behavioral tests

A set of behavioral tests were carried out while videos were recorded and analyzed via the ANY-maze (version 7.43; Stoelting, USA) [19].

Behavioral tests were separated by at least 24 h, and were performed over a period of 2–3 weeks. The order of behaviors was kept constant, with the least stressful paradigms being performed first, and the most stressful the last, as shown in Figs. 1A and 2E.

Rotarod test. The rotarod test was used to assess motor coordination and balance. It comprises three phases: adaptation, training, and testing. During adaptation, the mice were introduced to the rod rotating at a constant speed of 4 rpm and required to maintain their balance for 5 min. Following a 5 min rest period, the training involved three sessions with 5-min intervals, where the rotation speed gradually increased to 20 rpm over 5 min. Testing occurred 24 h post-training, with the rod accelerating to 40 rpm within 5 min. The latency to fall was recorded [19].

Von frey test. Mice were confined to a bottomless box (10 \times 10 cm) 30 cm above the ground and acclimated for 30 min. The hindfoot was stimulated with mechanical cilia (NC12775, North Coast) to observe paw withdrawal or licking responses [20]. Each mouse was tested three times per round,

with two responses considered successful. Two out of three successful rounds indicated the presence of a pain threshold.

Marble burying test. Corncob bedding was used to fill one-third of the cage (30 \times 5 \times 15 cm), with 18 black beads (1.5 cm diameter) evenly distributed. The mice were allowed to move freely for 10 min, and the number of beads that were buried by more than two-thirds of bedding was recorded.

Open field test (OFT). Locomotor activity was measured in an open field chamber (51 \times 47 \times 45 cm). Spontaneous activity was video recorded for 30 min after the mice were placed in the center of the chamber. The horizontal distance traveled and repetitive self-grooming behaviors (licking paws, washing face, scratching fur) were manually recorded [19].

Elevated plus maze (EPM). The EPM was positioned 50 cm above the ground and consisted of two closed arms (30 \times 5 \times 15 cm) and two open arms (30 \times 5 cm). The mice were placed in the central area facing an open arm and allowed to explore freely for 5 min. The time spent and the number of entries into the open arms were recorded.

Tube test. A long transparent tube (30 cm long, 2.5 cm diameter) was used to measure social dominance. The mice were acclimated by shutting in the tube for 2 min. During the test, two mice entered opposite ends and met in the center. The winner (the one pushing the other out of the tube) was recorded within 5 min to determine social dominance.

Homecage movement. Mice were placed in their homecage (30 \times 5 \times 15 cm), and movement was recorded for 10 min.

Barnes maze test (BM). Mice were placed on a round white platform (90 cm diameter) with eight holes, one with an escape box (target hole). Intensive light serves as an aversive stimulation to motivate escape. During the training phase, the mice explored until they found the escape hole via visual cues. In the test phase, the escape box was removed, and the time spent around the correct hole (T1) and incorrect holes (T2) was recorded. The spatial memory index was calculated as T1/T2.

Active/passive avoidance test. This test involves two stages: active avoidance and passive avoidance. In the active avoidance test, the mice were placed in a lightbox (1000 lux) and timed until they moved to a dark box. The training involved repeated electrical stimulation (0.1–0.7 mA) to the lightbox, with the escape latency recorded. The testing session was conducted without electrical stimulation. The procedure was repeated the next day as a passive avoidance test, with intensive electrical stimulation (0.7 mA) in the dark box.

Prepulse inhibition (PPI). The PPI of the acoustic startle response was measured via the startle/PPI system with a four-cage setup (Ugo Basile, VA). The mice were placed in a Plexiglas cylinder and acclimated in the PPI box for 40 min. Two stimulus types were used: a 40 ms burst of varying sound intensities (90, 100, 110, 120 dB) and a prepulse sound (20 ms, 70, 76, 85 dB) presented 100 ms before a 120 dB startle stimulus. The PPI percentage was calculated as follows: (1 - prepulse startle stimulus/startle response alone) \times 100% [21].

Forced swimming test (FST). The FST evaluates depression by placing mice in water (15 cm depth, 20–25°C). The mice were observed for 10 min, and parameters such as latency to immobility (stop struggling) and duration without struggling were recorded.

Tail suspension test (TST). The TST also detects depression by suspending a mouse via the tail using adhesive tape attached to a hook, preventing it from touching the ground. The mice were observed for 10 min, and the latency to immobility and duration of immobility were recorded.

Spontaneous fine behavior test. Mice were placed in a black, circular arena (44 cm in diameter, 36 cm in height) for 1 h to explore freely, and their behavior was recorded via a depth camera (Kinect 2, Microsoft). The interior surface of the arena was nonreflective to prevent image distortion, and red light was used for illumination during recording. Between sessions, the cylinder was cleaned with 75% ethanol to avoid cross-contamination. The behavioral data were processed via a custom-built Python pipeline. Mouse position, orientation, and body shape were extracted from the raw depth data via

Table 1. Primer sequences for genotyping.

Primer	Sequence	Band Size
Shank3 P1	TGG ATC CTA GCT CAC CCT TAG	WT: 224 bp
Shank3 P2	CTC TCT CCG AGC AGG CAC T	Mutant: 300 bp

custom tracking software. The 3D image of each mouse was then aligned following a previously established motion sequencing. Mouse behavior recording and analysis were performed using the motion sequencing (MoSeq) pipeline (Moseq2, version v1.3.1) [22]. Initial depth images were denoised by resampling and applying background subtraction, with the background generated from the median of the first 1000 frames. The time series of the aligned images were sampled at a rate of 30 frames per second [23].

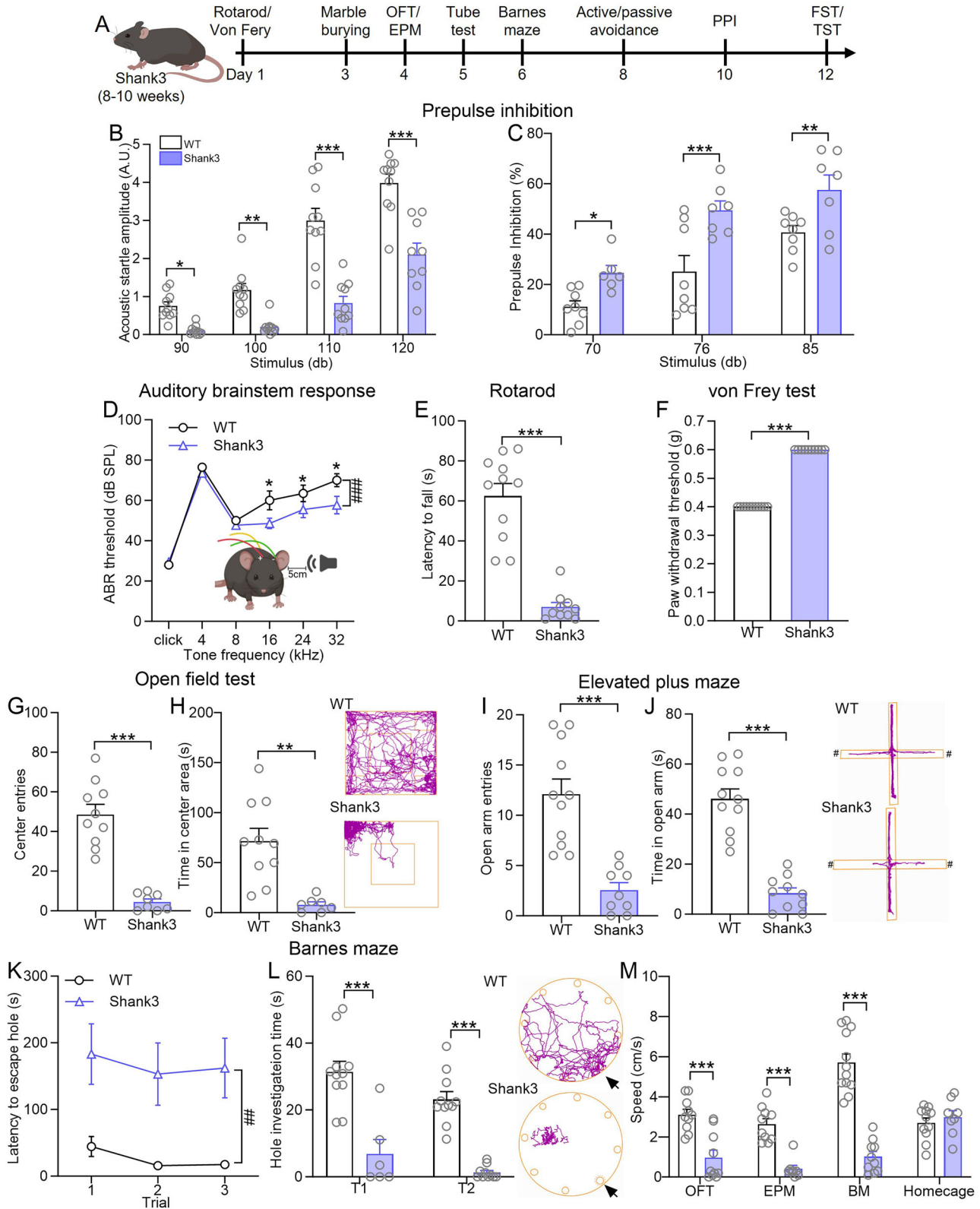


Fig. 1 Deficits in sensory gating, motor function, pain perception, and severe anxiety of homozygous R1117X Shank3 mice. **A** Schematic timeline of behavioral experiments. OFT open field test, EPM elevated plus maze, BM Barnes maze test, PPI prepulse inhibition, FST forced swimming test, TST tail suspension test. **B, C** Bar graph of the acoustic startle amplitude **B** and prepulse inhibition percentage **C** in wild-type (WT, $n = 8$) and homozygous R1117X Shank3 mice (Shank3, $n = 7$) mice during the PPI test (acoustic startle: $F_{(3,72)} = 71.79$, $p < 0.0001$; PPI: $F_{(2,38)} = 25.37$, $p < 0.0001$, RM two-way ANOVA). **D** Line chart of hearing thresholds in WT ($n = 10$) and Shank3 mice ($n = 11$) under varying sound frequencies in the auditory brainstem response (ABR) test ($F_{(5,59)} = 80.63$, $p < 0.0001$, RM two-way ANOVA). Inset: diagram of ABR detection. **E** Bar graph of latency to fall in WT ($n = 11$) and Shank3 ($n = 10$) mice during the rotarod test ($p < 0.0001$, Mann-Whitney test). **F** Bar graph of the paw withdrawal threshold in the Von Frey test ($p < 0.0001$, t test). **G** and **H** Bar graphs of number **G** and time **H** of entries into the central area of the OFT in WT ($n = 10$) and Shank3 ($n = 8$) mice (number: $p < 0.0001$; time: $p = 0.0002$, Mann-Whitney test). Insets: representative movement tracks in the OFT. **I** and **J** Bar graphs of the number **I** and time **J** entries into the open arms of the EPM in WT ($n = 11$) and Shank3 ($n = 10$) mice (number: $p < 0.0001$, Mann-Whitney test; time: $p < 0.0001$, t test). Insets: representative movement tracks in the EPM. **K** Line chart of escape latency to the correct hole of WT ($n = 10$) and Shank3 mice ($n = 9$) in the BM ($F_{(1,18)} = 14.27$, $p = 0.0014$, RM two-way ANOVA). **L** Bar graph of time spent exploring correct (T1) and incorrect (T2) holes ($F_{(1,34)} = 6.228$, $p = 0.0176$, RM two-way ANOVA). Insets: representative movement tracks in the BM, with arrows indicating the correct hole. **M** Bar graph of the speed during the OFT, EPM, BM and homecage of WT ($n = 10$) and Shank3 ($n = 9$) mice (OFT: $p = 0.0002$, Mann-Whitney test; EPM: $p = 0.0003$, Mann-Whitney test; BM: $p < 0.0001$, t test). Data are presented as the means \pm SEMs. $\#\#p < 0.01$, $\#\#\#p < 0.001$ by RM two-way ANOVA; $*p < 0.05$, $**p < 0.01$, $***p < 0.001$ by t test or Tukey's *post hoc* test of RM two-way ANOVA. See also supplementary Fig. 1 and 2.

MoSeq analysis of fine behavior is the unsupervised machine learning of behavioral videos by applying deep learning algorithms. The behavior of mice was segmented and then extracted to multiple behavior syllables. A syllable similarity dendrogram was generated to demonstrate the kinematic relationships among observed syllables. Run the generate dendrogram cell of the MoSeq pipeline will generate a hierarchically sorted dendrogram, within which the Voor Hees hierarchical clustering algorithm was used. The distance metrics that are used to identify kinematic similarities are based upon the matrix autoregressive computed as part of the MoSeq modeling step.

Homecage food self-administration. To assess operant behavior in mice, we utilized the feeding experimentation device version 3 (FED3) [24], an automated, home-cage-based system designed to monitor food self-administration. The mice were placed in their homecages, where they had continuous access to the FED3 device, allowing for training in a naturalistic environment without stress-induced factors from handling or removal. The device was programmed such that a nose-poke on the active port (left) triggered a combined tone and light as a conditioned stimulus, followed by the delivery of a 20 mg chocolate-flavored sucrose pellet (TestDiet). Nose-pokes on the inactive port (right) were logged but produced no consequences, providing a measure of exploratory or non-reward-seeking behavior. The training was conducted under a fixed ratio 1 (FR1) schedule, meaning that each successful nose-poke on the active port resulted in one pellet being dispensed. This schedule was used for task acquisition to establish the association between the active port and the reward.

Morris water maze (MWM). The MWM was conducted using a circular pool (120 cm in diameter), divided into four quadrants (I, II, III, and IV), with distinct visual cues on the wall of each quadrant [25]. The water temperature was maintained between 21–22 °C, and titanium dioxide was added to maintain water turbidity. The experiment consisted of three phases: adaptation, training, and testing. Mice were placed into the maze while facing the wall and allowed free movement for 60 s. The time, speed, and distance traveled to locate the platform were recorded. **Adaptation (visible platform):** The water level was set 1 cm below the platform (20 cm high, 5 cm in diameter), with a small flag placed on the platform. Mice were placed into the maze from 5 different entry points. **Training (hidden platform):** The platform was placed in a fixed position of quadrant III, with the water level raised 1 cm above the platform to ensure it was submerged. Upon reaching the platform, mice remained on the platform for 30 s. If the mice failed to locate the platform, they were gently guided to the platform and allowed to stay for 30 s. The training phase lasted for 4 days, with 5 different entry points on each day. **Testing:** The platform was removed. Mice were placed into the maze from quadrant I.

Auditory brainstem response (ABR). Mice were anesthetized via intraperitoneal injection of tribromoethanol (0.2 mL/10 g, M2910, Nanjing Aibei Biotechnology Co.). Anesthesia was considered adequate when there was no contraction upon pinching the hind limbs. A thermostatic heating blanket was used to maintain the animals' body temperature at (38 ± 1) °C during ABR recordings. The loudspeaker (MF1, TDT, USA) was positioned 5 cm from the left ear of the animal (Fig. 1D). To ensure accurate stimulation frequency and intensity, the sound-generating system (RZ6, TDT, USA) was calibrated before each experiment using a

research-grade microphone (Model 2850, B&K, Denmark). The click stimulus began at 90 dB and was decreased in 10 dB steps until the threshold was reached. Pure tone stimuli at frequencies of 4, 8, 16, 24, and 32 kHz were also tested [26]. Near-threshold responses were further tested in 5 dB increments, with each test repeated twice to finalize the auditory threshold.

Histology

The mice were anesthetized intraperitoneally (i.p.) with urethane (1 g/kg) before cardiovascular perfusion and brain extraction. The brain was fixed in 4% paraformaldehyde (PFA) overnight and then transferred to a 30% sucrose solution for 48 h before cryoprotection. Tissues were embedded in optimal cutting temperature (OCT) compound (Neg-50, EpreDia) and sectioned into 50 μ m slices via a cryostat (NX-50 Cryostar). The sections were washed in PBS and stained with Nissl stain (G1430, Solarbio). The staining involved immersion in tar violet for 20 s at room temperature, followed by rinsing in distilled water (ddH₂O) and tar violet differentiation solution for 20 s. The sections were dehydrated via an ethanol series (70, 80, 95, and 100%) for 60 s each, cleared in xylene for 60 s, and mounted with neutral resin. Imaging was performed via an inverted microscope (Axio Observer 7, ZEISS). The thickness, cell diameter, and number of cells in the dentate gyrus (DG), CA3, and CA1 regions of the hippocampus, cortex, and basolateral amygdala (BLA) were measured via Imaris (version 9.0.1; Oxford Instruments, GBR) [27].

Quantitative real-time PCR (qPCR)

After the behavioral tests, the hippocampal tissue from 8- to 10-week-old mice was dissected for RNA extraction via TRIzol (EC521, TransGen Biotech) following the manufacturer's protocol. Complementary DNA (cDNA) was synthesized via TransScript® All-in-One First-Strand cDNA Synthesis SuperMix (AQ601, TransGen Biotech). qPCR was carried out on a CFX Connect system (Bio-Rad) with SYBR Green. The primers used for the genes studied are listed in Table 2. The qPCR conditions were as follows: 50 °C for 2 min, 95 °C for 20 s, then 40 cycles of 95 °C for 1 s and 60 °C for 20 s. Relative mRNA expression levels were calculated via the 2- $\Delta\Delta$ Ct method and normalized to those of GAPDH [28].

Western blotting

Hippocampal tissue was lysed in cold RIPA buffer supplemented with protease inhibitor (R0020, Solarbio). After homogenization and centrifugation at 700 \times g for 7 min, the supernatant was collected and centrifuged again at 100,000 \times g for 15 min at 4 °C. The protein concentration was determined via a BCA protein assay kit (PC0020, Solarbio). Protein samples (20 μ g) were separated by 10% SDS-PAGE and transferred onto polyvinylidene fluoride membranes. The membranes were blocked with 5% nonfat milk for 1 h at room temperature and incubated overnight at 4 °C with primary antibodies against GluN1 (AF6406, Affinity, 1:1000), GluN2A (DF7955, Affinity, 1:1000), GluN2B (AF6426, Affinity, 1:1000) and GluA1 (abs136161, Absin, 1:1000). A secondary antibody (S0001, Affinity, 1:10000) was applied for 1 h at room temperature. The blots were visualized via a Bio-Rad Imager (FUSION FX EDGE, Vilber Smart Imaging), and the protein levels were normalized to those of GAPDH (KC-5G5, Aksomics, 1:10000) [29].

Table 2. Primer sequences for qRT-PCR.

Gene	Forward primer sequences (5' to 3')	Reverse primer sequences (5' to 3')
<i>Grin1</i>	CATCGGACTTCAGCTAATCA	GTCCCCATCTCATTGAATT
<i>Grin2a</i>	GGCTACAGAGACTTCATCAG	ATCCAGAAGAAATCGTAGCC
<i>Grin2b</i>	TTAAACAACCTCCGTACCTGTG	TGGAACTTCTGTCACTCAG
<i>Gria1</i>	GCCTTAATCGAGTTCTGCTA	GAATGGATTGCATGGACTTG
<i>Gria2</i>	AGCCTATGAGATCTGGATGT	GAGAGAGATCTTGGCGAAAT
GAPDH	AAGGTGGTGGAGAGGGAAT	TCAAACCATTTGGCACACGAC

Electrophysiology

The mice were deeply anesthetized with isoflurane and transcardially perfused with ice-cold artificial cerebrospinal fluid (ACSF) before decapitation, as described previously [30]. The ACSF contained the following (in mM): NaCl 124, KCl 2.8, NaH₂PO₄ 1.25, NaHCO₃ 26, D-glucose 10, vitamin C 0.4, pyruvate-Na 2, lactate-Na 2, CaCl₂ 2.0, MgSO₄ 1.2, pH = 7.2–7.4, 295 mOsmol [25]. The hippocampi were removed and cut into acute coronal slices (400 μm thick) via a vibratome (VT1200S, Leica Microsystems, Germany) in ACSF bubbled with 95% O₂ and 5% CO₂. The slices were incubated in oxygenated ACSF for 1 h at 32 °C. The field excitatory postsynaptic potentials (fEPSPs) were evoked by stimulation of the Schaffer collateral/commissural pathways and recorded in the CA1 area of the hippocampus via pipettes (3–4 MΩ) filled with ACSF, and perfused with 95% O₂ + 5% CO₂ saturated ACSF (3 mL/min). Input-output (I/O) curves were generated by plotting the fEPSPs slope versus current stimulation. Paired-pulse responses were measured with varied interstimulus intervals (ISIs) and are expressed as the ratio of the average responses to the second stimulation pulse to the first stimulation pulse. After a 10-min stable baseline, theta burst stimulation (TBS) was given to induce long-term potentiation (LTP). TBS consisted of two trains of stimuli (at 20 s intervals), with each train composed of five bursts of four pulses at 100 Hz separated by 200 ms. Data acquisition was performed with PatchMaster v2.73 software (HEKA Electronic, Germany), digitized at 10 kHz, and filtered at 3 kHz.

Statistics

GraphPad Prism 8.3.0 (GraphPad Prism Software) was used for statistical analysis. All the data are expressed as the means ± standard errors of the means (SEMs). The Shapiro-Wilk test was used to assess normality. To test for equality of variances, either the F-test or the Brown-Forsythe test was applied. Outliers were identified using either the ROUT method or Grubbs' test. For data that did not meet these assumptions, we used the Mann-Whitney U test or mixed-effects analysis, as appropriate. Experiments with two groups were analyzed via t tests (unpaired). Experiments with more than two groups were subjected to two-way ANOVA (regular or repeated measures (RM)), followed by Tukey's post hoc tests for multiple comparisons when significant ANOVA effects were detected ($p < 0.05$). The pound sign indicates a significant difference between groups according to two-way ANOVA (# $p < 0.05$, ## $p < 0.01$, ### $p < 0.001$). An asterisk indicates statistical significance for the t test (unpaired) or Tukey's post hoc test of two-way ANOVA (* $p < 0.05$, ** $p < 0.01$, *** $p < 0.001$).

RESULTS

Deficits in sensory gating, motor function, and pain perception in homozygous R1117X *Shank3* mice

Point mutations in the *Shank3* gene, specifically at the beginning of exon 21, result in the substitution of arginine (CGG) with a stop codon (TGA) (Figure S1A). To generate homozygous *Shank3* point mutant mice, *Shank3* homozygous mice were bred with a 1:3 male-to-female ratio (Figure S1B). Genotyping via tail clipping confirmed the homozygous *Shank3* point mutation (*Shank3*) at 300 bp, while WT mice exhibited a 224 bp band (Figure S1C). At 8 weeks of age, no significant differences in brain size (Figure S1D) and body weight (Figure S1E, F) were observed between *Shank3* mutant and WT mice, suggesting that the R1117X mutation does not affect growth.

Since the *Shank3* R1117X mutation was initially identified in schizophrenia patients [17], and PPI has been suggested as an important measurement for schizophrenia [31], we first assessed

the sensorimotor gating by using PPI in *Shank3* R1117X mutant mice. These mice exhibited marked deficits in acoustic startle responses: although startle responses increased with sound intensity, they remained significantly lower than those of WT mice (Fig. 1B). This suggests that *Shank3* mutant mice are less responsive to sound stimuli. Interestingly, when a low-decibel pre-stimulus was followed by a high-decibel sound, *Shank3* mutants showed significantly suppressed startle response, resulting in an increased PPI (Fig. 1C), indicative of abnormal sensorimotor gating.

To test whether deficits in startle responses are caused by potential hearing abnormalities, ABR testing [32] was conducted. No significant threshold differences were observed in the click-stimulation between *Shank3* mutants and WT mice (Fig. 1D). However, in the pure-tone test, while there were no significant differences in thresholds for low-frequency sounds (4 and 8 kHz), *Shank3* mutants exhibited significantly lower thresholds for high-frequency sounds (16, 24, and 32 kHz) compared to WT mice (Fig. 1D). This suggests that *Shank3* mutants have normal hearing responses to regular clicks and low-frequency sounds, but are more sensitive to high-frequency sounds.

Meanwhile, motor coordination was evaluated using the rotarod test, which assesses balance and motor coordination [33]. *Shank3* mutant mice spent significantly less time on the rotating rod than WT mice (Fig. 1E), indicating motor coordination deficits, which aligns with previous reports [34]. The von Frey test, used to evaluate mechanical allodynia, was also performed to assess pain sensitivity [20] in *Shank3* mutants. The results indicated that *Shank3* mice have a higher mechanical pain threshold compared to WT mice (Fig. 1F), suggesting reduced sensitivity to pain.

Together, these results demonstrate that *Shank3* mutant mice exhibit significant abnormalities in sensory processing, motor function, and pain perception.

Shank3 mutant mice exhibit severe anxiety in novel environments

To characterize the behavioral phenotypes of *Shank3* mutant mice, a series of behavioral tests were conducted (Fig. 1A). A previous study reported anxiety-related behaviors and stereotypes in *Shank3* mutant mice, such as those associated with the *InsG3680* mutation [17]. To further assess anxiety-like behaviors in R1117X *Shank3* mice, we employed the OFT and the EPM. In the OFT, *Shank3* mice significantly fewer entries (Fig. 1G) and spent less time in the central area (Fig. 1H) compared to WT mice. Similarly, in the EPM, *Shank3* mice showed fewer entries (Fig. 1I) and spent less time in the open arms (Fig. 1J) than WT mice. Furthermore, *Shank3* mice exhibited reduced overall movement in both the OFT and EPM, as indicated by the tracks (Fig. 1H and J).

To evaluate learning and memory, we performed the BM test. During the training sessions, *Shank3* mice took significantly longer time to find the escape hole than WT mice (Fig. 1K). Notably, the latency to find the escape hole in *Shank3* mice did not decrease with repeated training trials, and the escape latency was almost equivalent to the total duration of the experiment. Additionally, *Shank3* mice spent significantly less time exploring both the

correct escape hole (T1) and incorrect holes (T2) compared to those of WT mice (Fig. 1L). Trajectory track revealed that Shank3 mice exhibited limited activity and exploration, suggesting that they were not engaging in the task adequately. This behavior does not suggest a general cognitive deficit but rather indicates a lack of movement and ineffective learning, possibly due to high anxiety. Shank3 mice did not exhibit clear avoidance behavior but had less movement in response to strong light stimuli.

The movement speed of Shank3 mice was measured across multiple behavioral assays, including the OFT, EPM, BM, and homecage. In contrast to WT mice, which showed a significant increase in movement speed in response to strong light stimulation of the BM, Shank3 mice only exhibited normal movement in the homecage. In the novel environments of the OFT, EPM, and BM, their movement speed was significantly reduced (Fig. 1M).

Additionally, Shank3 mice displayed less grooming behavior at 15 min in the OFT (Figure S1L) but engaged in significantly more grooming at 60 min (Figure S1M). Shank3 mice buried significantly fewer marbles than WT mice (Figure S1N) in the marble burying test, but had a higher success rate in the tube test (Figure S1G). However, these findings should not be interpreted as indicating stereotyped behaviors or social advantages. The reduced marble burying and tube test performance are more likely reflective of the reduced activity and increased anxiety of Shank3 mice in novel environments.

In the FST and TST, which evaluated the depressive-like behavior (Figure S1H–K), Shank3 mice showed a significantly shorter latency to immobility (Figure S1H and J) but did not differ from WT mice in terms of total immobility time (Figure S1I and K).

Collectively, these behavioral findings indicate that R1117X Shank3 mice exhibit high levels of anxiety in novel environments, which is reflected in their reduced activity. These results underscore the role of Shank3 in regulating anxiety-related behaviors, particularly in response to environmental novelty.

Mild anxiety and cognitive deficits of heterozygous Shank3 mutant mice

To determine whether the observed abnormalities were specific to homozygous Shank3 mutant mice, we conducted a series of behavioral assessments on Shank3 heterozygous (Shank3-Het) mice. In the rotating rod test, Shank3-Het mice exhibited a slightly decreased drop latency compared to WT mice, but without a statistically significant difference (Figure S2A). Von Frey testing revealed no significant difference in mechanical pain thresholds between Shank3-Het and WT mice (Figure S2B), indicating unaltered pain perception.

Grooming behavior in Shank3-Het mice was slightly increased compared to WT mice, but without a significant difference (Figure S2C). In the marble burying test, Shank3-Het mice buried fewer marbles than WT mice (Figure S2D), suggesting an absence of stereotyped behaviors. Interestingly, Shank3-Het mice had a significantly higher success rate in the tube test (Figure S2E). For the movement, Shank3-Het mice did not show abnormalities in speed during the OFT, EPM, or homecage environments. However, their movement speed was reduced in the BM (Figure S2N).

For the anxiety-like behavior, Shank3-Het mice had fewer entries and less time spent in the center area of OFT than those of WT mice (Figure S2F and G). A similar trend was observed in the EPM, where Shank3-Het mice made fewer entries into the open arms compared to WT mice (Figure S2H), although there was no significant difference in the time spent on the open arms (Figure S2I).

For the depressive-like behavior, Shank3-Het mice exhibited significantly shorter immobility time in FST and TST compared to WT mice (Figure S2K and M), without difference in the latency to immobile (Figure S2J and L), suggesting no depression-like behaviors in Shank3-Het mice.

For cognitive function, Shank3-Het mice had similar escape latencies during the training sessions of the BM (Figure S2O), as well as memory index (T1/T2) during test session compared to those of WT mice (Figure S2P), indicating normal working memory in Shank3-Het mice. In the active avoidance test (L-D), Shank3-Het mice showed a much higher baseline latency to avoid the light stimulus compared to WT mice (Figure S2Q), but the escape latency of Shank3-Het mice was comparable to that of WT mice after foot shock training (Figure S2Q and R). In the passive avoidance test (D-L), Shank3-Het mice exhibited consistently longer escape latency when exposed to strong stimuli (Figure S2S) and during the D-L test (Figure S2T) compared to those of WT mice, indicating learning and memory deficits to aversive electric shock.

Overall, these findings suggest that Shank3 R1117X heterozygous mutant mice exhibit anxiety-like behaviors, learning and memory deficits. However, these abnormalities are less pronounced compared to those observed in homozygous Shank3 mutants.

Learning and memory deficits in Shank3 mice

Shank3 mice display heightened anxiety in novel environments and reduced sensitivity to pain and foot shock, which complicates the interpretation of behavioral outcomes from traditional tasks such as the BM test. We further used the shuttle box test to assess the cognitive function [35]. Shank3 mice exhibited longer latencies to avoid a low-intensity electrical shock (0.1 mA, Fig. 2A) compared to WT mice. Avoidance behavior was only observed at higher current intensities (above 0.3 mA). Even in the absence of foot shock during test, Shank3 mice displayed increased escape latency (Fig. 2B), suggesting memory deficits related to the previous foot-shock stimulus. In the passive avoidance test, where mice received an electric foot shock in the dark box, Shank3 mice displayed avoidance behavior to that of WT mice under strong shock (0.7 mA) conditions (Fig. 2C). However, Shank3 mice consistently exhibited significantly longer escape latency throughout the test (Fig. 2C), suggesting potential impairments in learning. Moreover, Shank3 mice spend significantly longer time to shuttle both in the D-L test and L-D test (Fig. 2D), indicating memory deficits. However, the observed learning and memory deficits in the shuttle box test would be affected by the observed novel environment-induced anxiety or less sensitivity to pain in Shank3 mice.

To mitigate the anxiety and pain perception issues, we further employed the FED3 system [24] a home-cage-based food self-management task in conjunction with the MWM (Fig. 2E). In the FED3 task, WT mice quickly learned to nose-poke the correct port for a food reward within 3 days under FR1 schedule. In contrast, Shank3 mice required 7–9 days to complete the task (Fig. 2F–H). Throughout the training, Shank3 mice consistently made fewer correct nose-pokes to the designated port compared to WT mice (Fig. 2F). Interestingly, they also performed fewer incorrect nose-pokes (Fig. 2G), suggesting a reduced motivation to explore unfamiliar aspects of the environment, even in the familiar context of their homecage. During the first 7 days of training, Shank3 mice exhibited significantly lower correct nose-poke rates than WT mice (Fig. 2H), indicating learning deficits. However, by day 8, both groups reached comparable performance levels, suggesting that Shank3 mice eventually achieved similar memory retention. These findings highlight a pronounced deficit in the learning abilities of Shank3 mice, though their memory appears relatively unaffected once the task is learned.

In the MWM adaptation phase, Shank3 mice swam faster than WT mice (Fig. 2I), suggesting heightened anxiety and a greater tendency to flee in a novel environment. Despite this, Shank3 mice demonstrated significantly longer escape distances (Fig. 2J) to find the visible platform than WT mice, indicating impairments in learning function. Over the 4-day MWM training phase, the

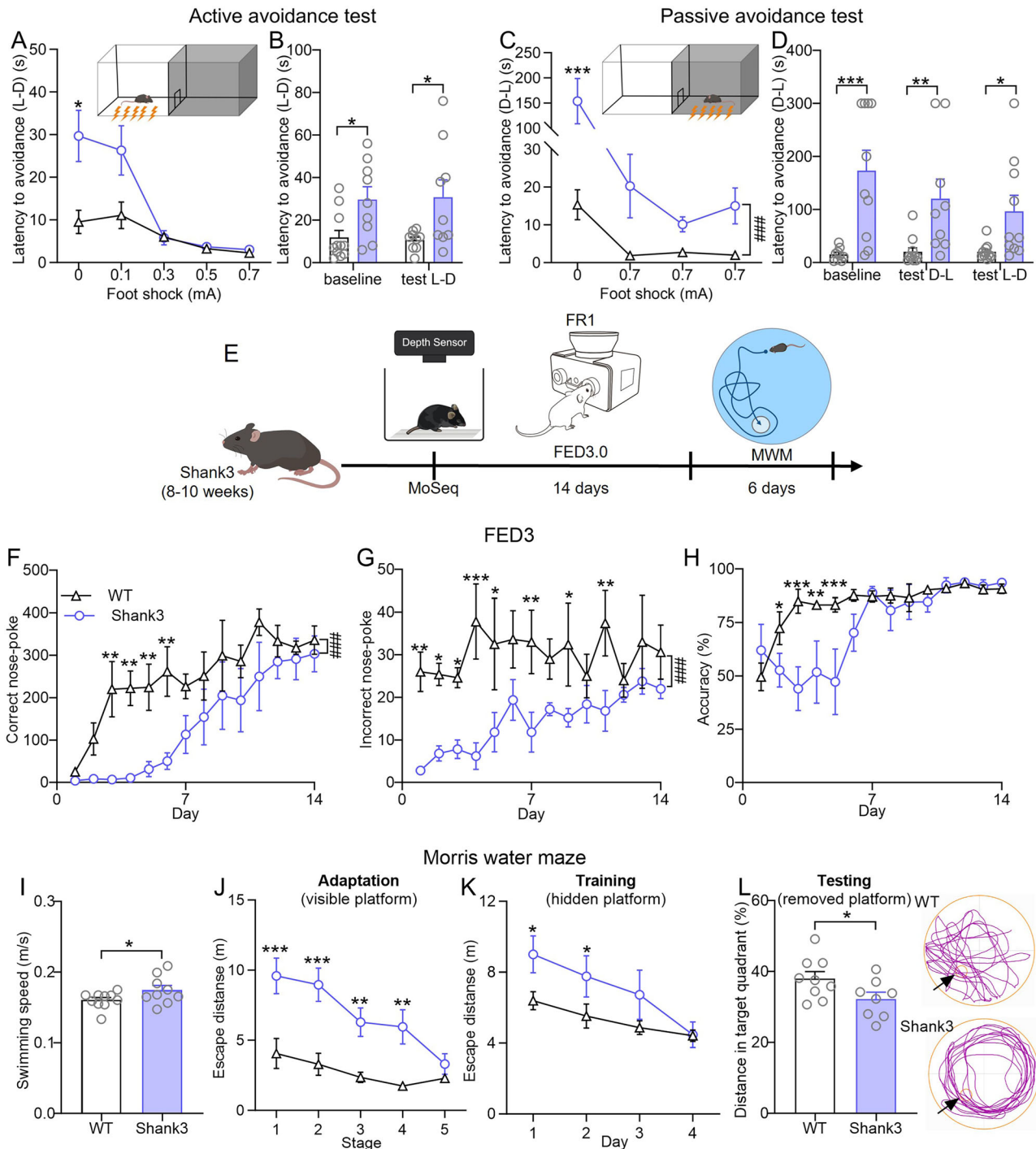


Fig. 2 Learning and memory deficits in Shank3 mice. **A** Line chart of escape latency to the dark box under varying electric shock intensities (0–0.7 mA) during the light to dark (L-D) active avoidance test in WT ($n = 10$) and Shank3 ($n = 9$) mice ($F_{(4, 92)} = 16.91, p < 0.0001$, RM two-way ANOVA). **B** Bar graph of latency from light box to the dark box at baseline and after 0.7 mA electric shock ($F_{(1, 34)} = 13.16, p = 0.0009$, RM two-way ANOVA). **C** Line chart of escape latency to the lightbox under fixed shock intensity (0.7 mA) during the dark to light (D-L) passive avoidance test ($F_{(3, 65)} = 13.39, p < 0.0001$, RM two-way ANOVA). **D** Bar graph of latency to shuttle at baseline and after foot shock ($F_{(1, 54)} = 30.96, p < 0.0001$, RM two-way ANOVA). **E** Schematic timeline of behavioral experiments. **F–H** Line charts of correct nose-poke **F**, incorrect nose-poke **G** and accuracy **H** in home-cage food self-administration of WT ($n = 5$) and Shank3 ($n = 5$) mice generated by feeding experimentation device version 3 (FED3) (correct nose-poke: $F_{(1, 109)} = 40.28, p < 0.0001$; incorrect nose-poke: $F_{(1, 111)} = 60.62, p < 0.0001$; accuracy: $F_{(1, 112)} = 15.13, p = 0.0002$, RM two-way ANOVA). **I** Bar graph of swimming speed during the adaptation (visible platform) phase of Morris water maze (MWM) in WT ($n = 10$) and Shank3 ($n = 11$) mice ($p = 0.0349$, t test). **J** and **K** Line charts of escape distance to the platform during adaptation **J** and training phase (hidden platform, **K**) (adaptation phase: $F_{(1, 19)} = 21.02, p = 0.0002$; training phase: $F_{(1, 19)} = 0.8269, p = 0.3746$, RM two-way ANOVA). **L** Bar graph of percentage of swimming distance in target quadrant (III) during the testing phase ($p = 0.0324$, t test). Insets: representative movement tracks in the testing phase of MWM test. Arrows indicate the location of the removed escape platform. Data are presented as the means \pm SEMs. ### $p < 0.001$ by RM two-way ANOVA; * $p < 0.05$, ** $p < 0.01$, *** $p < 0.001$ by t test or Tukey's *post hoc* test of RM two-way ANOVA. See also supplementary Fig. 2.

escape distance to find the hidden platform decreased with continued training both in WT and Shank3 mice, yet still significantly longer in Shank3 compared to those of WT mice (Fig. 2K), especially on the 1st and 2nd training sessions, indicating persistent learning deficits. In the testing phase of MWM, Shank3 mice spent significantly less time in the target quadrant (III) compared to WT mice (Fig. 2L). The trajectory further revealed that WT mice spent more time in the target quadrant, whereas Shank3 mice exhibited more circular, directionless behaviors, suggesting they failed to form a clear memory of the platform location.

The results from both the FED3 and MWM tasks provide a more accurate assessment of the learning and memory impairments in Shank3 mice. Collectively, these findings underscore that homozygous Shank3 mutations result in substantial cognitive deficits, particularly in learning.

Abnormal spontaneous fine behaviors in Shank3 mice

To characterize the spontaneous behaviors of Shank3 mice precisely, we recorded their activity over 60 min and analyzed it via the MoSeq platform [23]. By training a classifier on different behavioral metrics (position, velocity, combined 2D measures (referred to as “scalar”), and MoSeq data), MoSeq demonstrated an accuracy of 83.8% in distinguishing Shank3 mice from WT controls (Fig. 3A, B). This confirms MoSeq’s capacity to objectively and accurately compare behavioral patterns between groups.

The model identified 71 unsupervised behavioral clusters (Fig. 3C), which were ranked based on their differences between Shank3 mice and WT mice. The behaviors to the left of the red dashed line represent those upregulated in Shank3 mice, whereas those to the right of the blue dashed line indicate downregulated behaviors. These 71 behaviors were grouped into eight distinct behavioral subtypes (Fig. 3D), including grooming, head-turning with movement, head-down movement, head-up stepping, back arching, immobility, upright, and head-up movement (Table 3).

Compared with WT mice, Shank3 mice presented significant differences in five of these eight subtypes: three behaviors increased (grooming, immobility, head-up movement) and two decreased (head-down movement, upright) (Fig. 3E). The most pronounced changes were observed in the “head-down movement” subtype (subtype 3), which was notably decreased, whereas “immobility” (subtype 6) was the most upregulated (Fig. 3E).

These findings highlight substantial alterations in spontaneous behavior in Shank3 mice, including heightened stereotypy, increased anxiety-like behaviors, and pronounced motor impairments.

Morphological changes in the hippocampus of Shank3 mice

The hippocampus, a critical brain region for learning and memory, is essential for the formation, consolidation, and retrieval of memories [36]. *Shank3* is highly expressed in the hippocampus [37]. Alterations in hippocampal structure are likely contributed to the learning and memory deficits observed in Shank3 mutant mice.

Nissl staining of the hippocampus revealed significant structural changes in the DG, CA3, and CA1 regions of Shank3 mice (Fig. 4A). Both the DG and CA3 regions exhibited increased thickness (Fig. 4C), as well as a marked increase in cell density (Fig. 4D). The cell diameter in the DG was significantly larger, while it decreased in the CA3 region (Fig. 4E). Notably, no significant change in thickness was observed in the CA1 region of Shank3 mice (Fig. 4A and C), but both cell density and cell diameter were increased in this region (Fig. 4D, E).

Previous studies have reported significant synaptic transmission defects in the prefrontal cortex (PFC) of Shank3 mice [17]. Consistent with this, Nissl staining of the cortex showed increased cell density but not diameter in Shank3 mice (Fig. 4B, D, E), suggesting that functional abnormalities in the cortex are accompanied by structural changes. In contrast, no such

morphological alterations were observed in the BLA, where cell number and diameter remained unchanged (Fig. 4B, D, E).

These hippocampal structural abnormalities in Shank3 mice are consistent with the observed behavioral deficits, supporting the idea that hippocampal alterations contribute to the cognitive impairments associated with *Shank3* mutations.

Synaptic transmission and plasticity deficits in the hippocampus of Shank3 mice

By observing the structural changes in the hippocampus, we further explored the changes in synaptic transmission and plasticity in the hippocampus via electrophysiological recordings of fEPSPs. fEPSPs were recorded in the CA1 region while electric stimulation was applied at the Schaffer collaterals from CA3.

Compared with those of WT mice, the I/O curves of the fEPSPs slopes at different current stimulations (0.2–0.5 mA) revealed pronounced suppression of fEPSPs slopes with various stimulation intensities (Fig. 5A, B), suggesting impaired basal synaptic transmission. The paired-pulse ratio (PPR) at various intervals was consistently lower in Shank3 mice than in WT mice (Fig. 5C). Further analysis of the PPR at 200 ms intervals revealed suppressed facilitation in Shank3 mice (Fig. 5D, E), indicating that short-term synaptic plasticity deficits affected presynaptic transmission in the mutant mice.

We further tested the LTP of synaptic transmission. Following a 10-min stabilization of fEPSPs recordings as a baseline, TBS was applied, and continuous recording was conducted for an additional 30 min. After TBS, the fEPSPs slope in Shank3 mice was temporarily potentiated but significantly lower than that in WT mice (Fig. 5F). Further analysis of fEPSPs slope changes at 20–30 min after TBS that weaker potentiation in Shank3 mice did not last longer than 30 min (Fig. 5G, H).

These results indicate that basal synaptic transmission, short-term facilitation, and LTP (both induction and maintenance) are suppressed in the hippocampus of Shank3 mice, which is consistent with the observed impairments in learning and memory.

Downregulation of glutamatergic receptors in the hippocampus of Shank3 mice

As excitatory glutamatergic receptors, including AMPA and NMDA receptors, are involved in the induction and maintenance of LTP [38], we further investigated the transcription and expression levels of these receptors in the hippocampus of Shank3 mice.

At the mRNA level, the levels of *Grin1*, *Grin2a*, *Grin2b*, and *Gria1* were significantly reduced in Shank3 mice (Fig. 6A). At the protein level, only GluN1 and GluA1 were significantly reduced in Shank3 mice (Fig. 6B, C). This reduction is consistent with observations in the striatum of Shank3 mice [17] and is linked to the R1117X mutation causing premature termination downstream of the codon. These data align with electrophysiological findings that Shank3 mutation suppressed both AMPA and NMDA receptors and triggered abnormal hippocampal synaptic function in mice.

DISCUSSION

This study focused on the behavioral, morphological, mechanistic, and molecular defects of Shank3 mice with the R1117X mutation. The Shank3 mice presented significant abnormalities, such as decreased motor and learning ability, and sensory gating deficits. Shank3 mice presented abnormal hippocampal morphology and increased hippocampal thickness and cell diameter. Electrophysiological results show impaired hippocampal synaptic plasticity in Shank3 mice. Shank3 mice also presented abnormal molecular expression, with reduced mRNA and protein expression levels of GluN1, GluN2A, and GluA1. Our

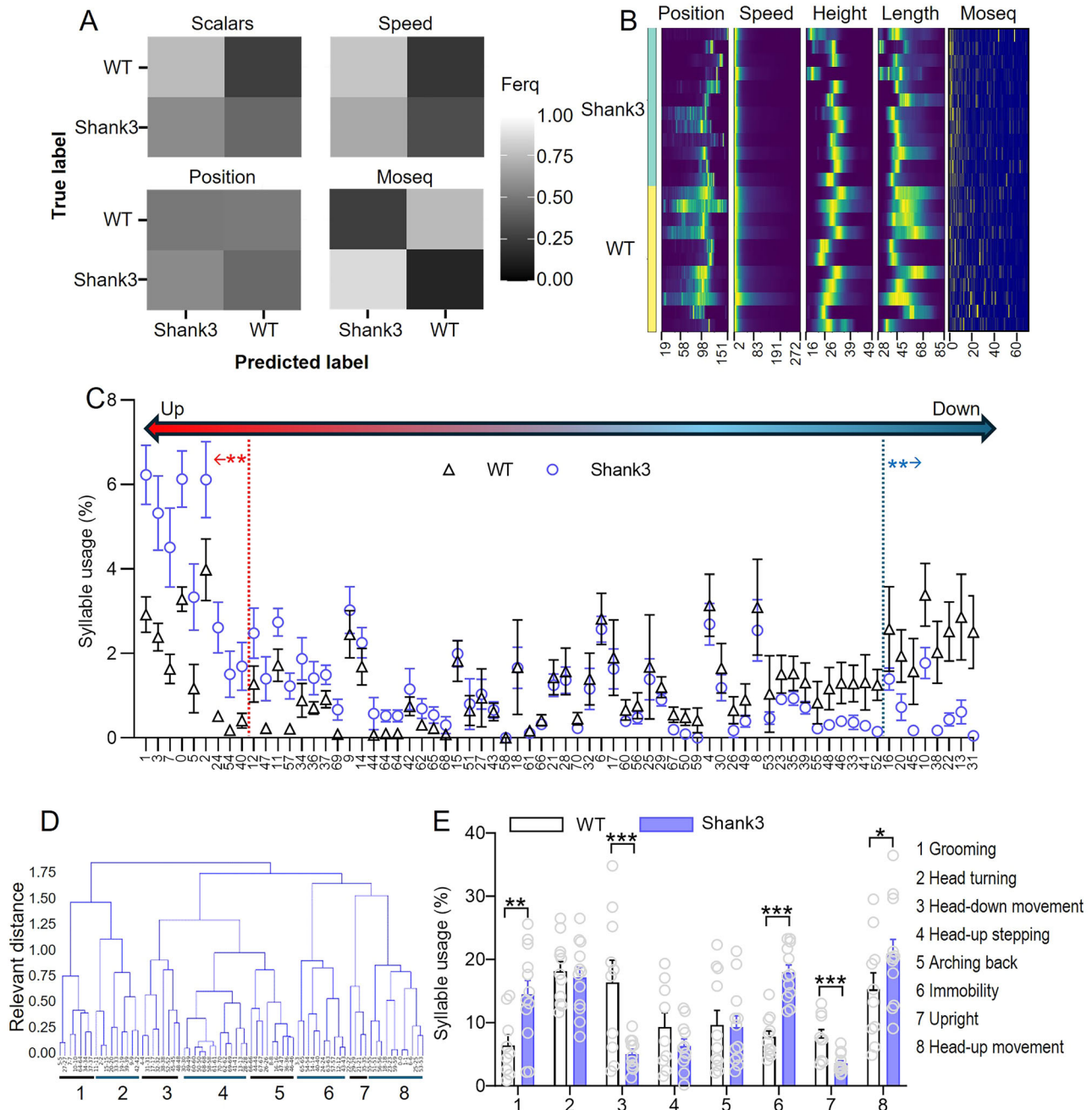


Fig. 3 Abnormal spontaneous fine behavioral features in Shank3 mice. **A** Normalized classification matrices highlight the performance of a linear classifier in distinguishing Shank3 mutant mice from WT mice. The classifiers were trained via various behavioral metrics, including position, speed, a combination of two-dimensional measures (“scalars”), or Motion Sequencing (MoSeq) syllables. The optimal classifier performance is indicated by white diagonal fields, with black fields representing frequencies of 1, reflecting perfect accuracy in distinguishing between the two groups. **B** Heatmaps of behavioral data derived from position, speed, height, length, and MoSeq syllables, comparing Shank3 and WT mice. **C** Plots of syllable usage with ordered based on the differences of changes. Increased syllables are on the left, whereas decreased on the right ($n = 10\text{--}12$ mice in each group; $F_{(71, 1496)} = 10.50$, $p < 0.0001$, RM two-way ANOVA). **D** Similarity dendrogram of the 71 syllables of MoSeq demonstrates hierarchical organization. **E** Histogram of syllable usage of eight key subtypes ($F_{(7, 158)} = 11.32$, $p < 0.0001$, RM two-way ANOVA). Data are presented as the means \pm SEMs. * $p < 0.05$, ** $p < 0.01$, *** $p < 0.001$ by Tukey’s *post hoc* test of RM two-way ANOVA.

results reveal the behavioral abnormalities and mechanisms in R117X Shank3 mice and expand the application direction of Shank3 mice in schizophrenia with severe cognitive deficits.

Spontaneous fine behavior

MoSeq is an ethologically inspired method that leverages three-dimensional machine vision and unsupervised machine

learning to decompose spontaneous mouse behavior into elemental modules known as “syllables.” This data-driven approach offers a detailed characterization of mouse behavior by revealing both the frequency of syllable usage and their transitions over time [22]. MoSeq outperforms traditional behavioral representations, particularly in tracking complex 3D behaviors, analyzing action sequences, and assessing

Table 3. Classification and description of spontaneous behavioral modules.

Behavior	Description
1 Grooming	Animal engages in cleaning its body by licking and scratching. Including face grooming and body grooming.
2 Head turning with movement	Animal turns its head in the direction of rotation.
3 Head-down movement	Animal lowers its head and moves forward.
4 Head-up stepping	Animal lifts its head while moving forward slowly.
5 Arching back	Animal arches its back by lowering its head and crouching.
6 Immobility	Animal stops moving abruptly, either while walking or at rest.
7 Upright	Animal stands on its hind legs with its back straight.
8 Head-up movement	Animal raises its head while moving forward.

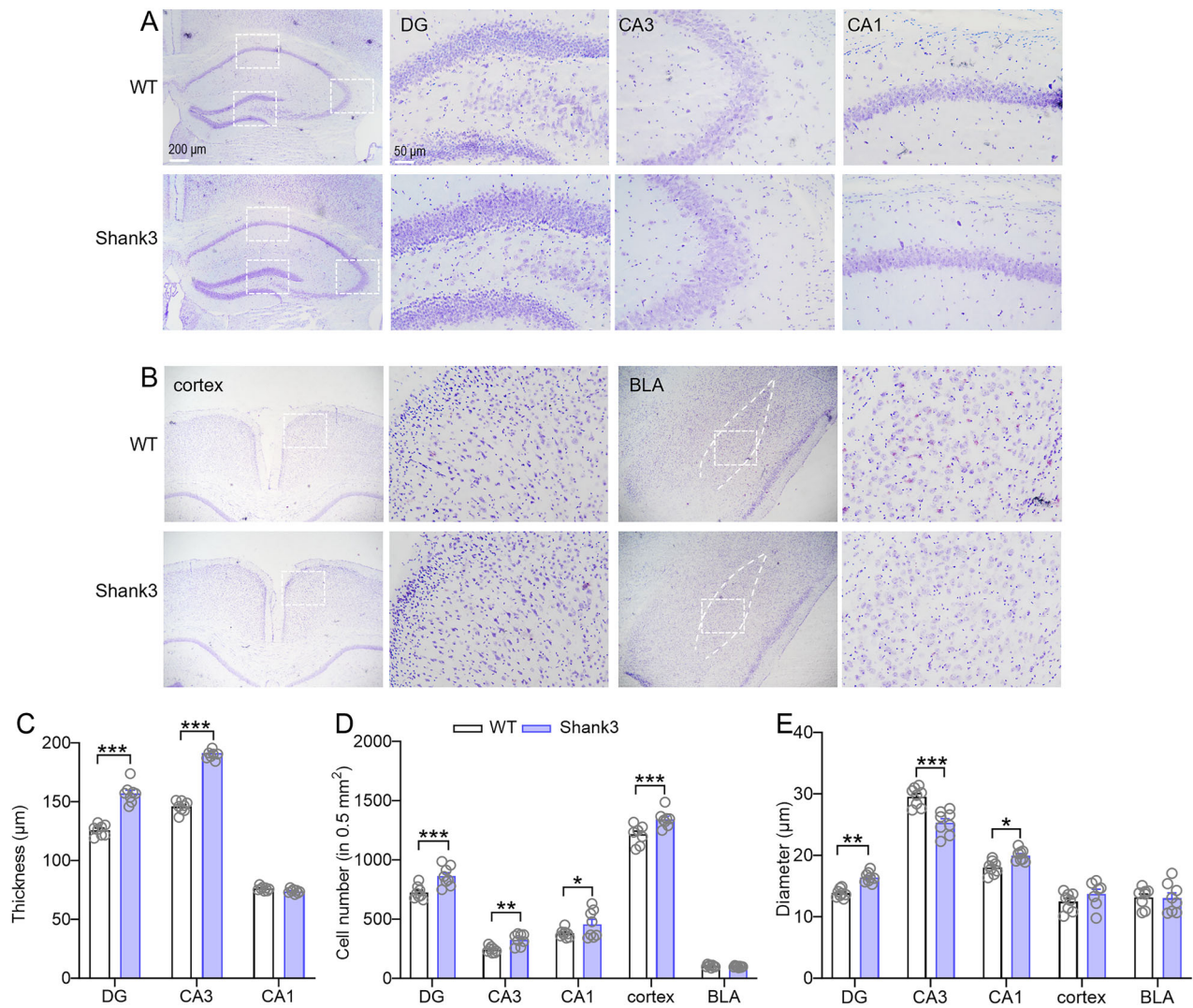


Fig. 4 Morphological changes in the hippocampus of Shank3 mice. **A** and **B** Representative Nissl staining images of the hippocampus **A**, cortex, and basolateral amygdala (BLA, **B**) with zoomed-in images of the dentate gyrus (DG), CA3, and CA1 regions, as well as cortex and BLA. Scale bars: 200 µm for low magnification, 50 µm for high magnification. **C** Bar graph of layer thickness in the hippocampal DG, CA3, and CA1 regions of WT and Shank3 mice ($n = 8$ slices from 4 mice in each group; DG: $p < 0.0001$; CA3: $p < 0.0001$; t test). **D** Bar graphs of cell number in high magnification images with an area of approximately 0.5 mm² in the DG, CA3, CA1, cortex, and BLA regions (DG: $p < 0.0001$; CA3: $p < 0.01$; CA1: $p = 0.0151$; cortex: $p < 0.001$; t test). **E** Bar graphs of cell diameter in the hippocampal DG, CA3, CA1, cortex, and BLA regions (DG: $p = 0.0013$; CA3: $p < 0.0001$; CA1: $p = 0.0145$; t test). Data are presented as the means \pm SEMs. * $p < 0.05$, ** $p < 0.01$, *** $p < 0.001$ by t test.

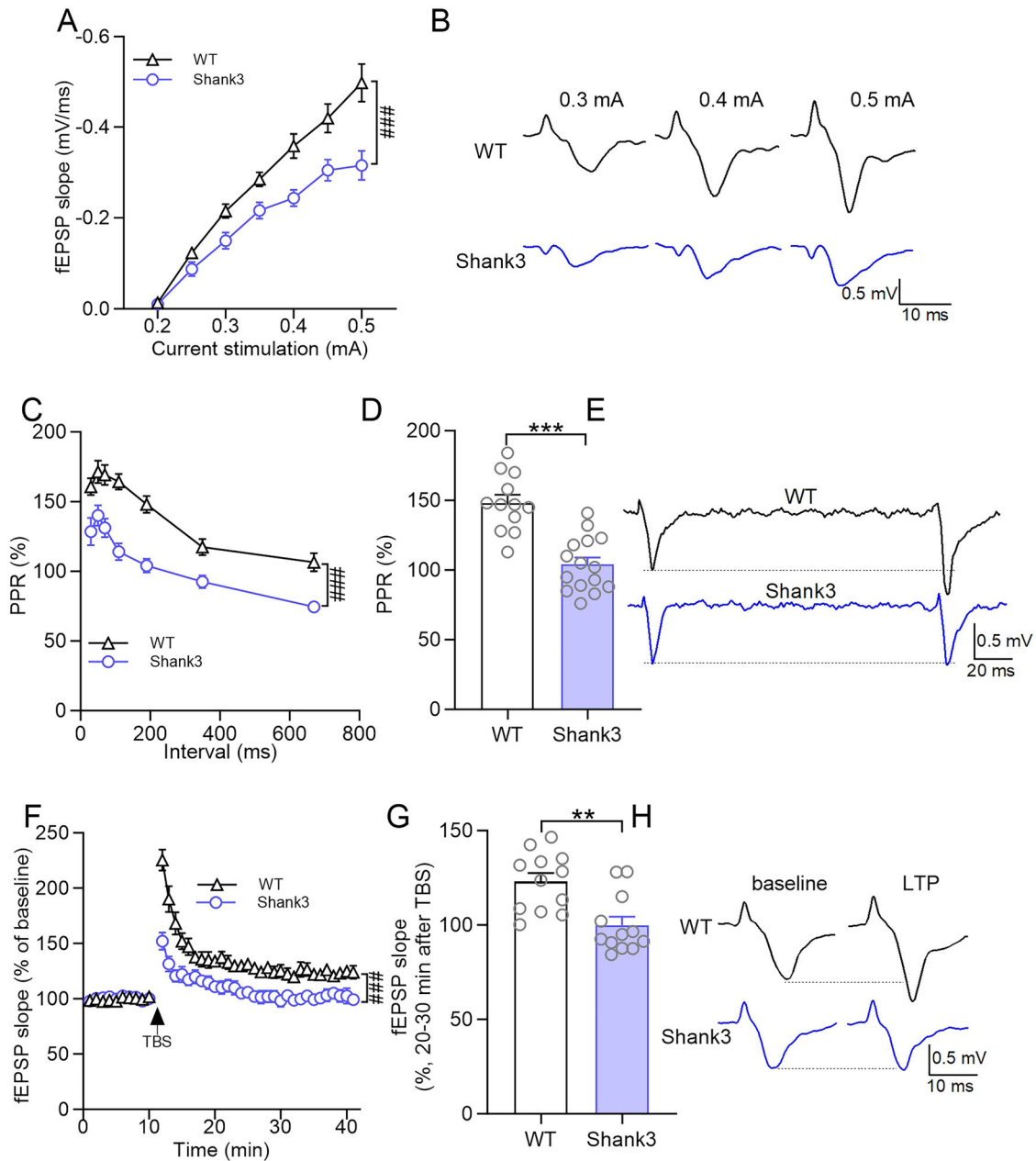


Fig. 5 **Suppressed hippocampal synaptic transmission and long-term potentiation in Shank3 mice.** **A, B** Line chart of input-output curves of field excitatory post-synaptic potentials (fEPSPs) slopes with different current stimulations in the CA3 to CA1 pathways of hippocampal slices from WT and Shank3 mice ($n = 12-14$ slices from 3-5 mice in each group; $F_{(6, 119)} = 6.793, p < 0.0001$, RM two-way ANOVA). **B**: representative fEPSP traces. **C** Line chart of the paired-pulse ratio (PPR) with different interpulse intervals ($n = 12-15$ slices from 3-5 mice in each group; $F_{(1, 26)} = 46.03, p < 0.001$, RM two-way ANOVA). **D, E** Bar graph of the PPR with an interpulse interval at 190 ms ($n = 13-15$ slices from 3-5 mice; $p < 0.0001$, t test). **E**: Representative traces with 200 ms inter-pulse intervals. **F** Normalized fEPSPs slope 10 min before and 30 min after long-term potentiation (LTP) induction with theta burst stimulation (TBS) ($n = 12$ slices from 3-4 mice in each group; $F_{(39, 828)} = 9.306, p < 0.0001$, RM two-way ANOVA). **G, H** Bar graph of the normalized fEPSPs slope at 30 min after LTP induction ($n = 12$ slices from 3-5 mice; $p = 0.0014$, t test). **H**: Representative traces 5 min before and 30 min after LTP induction. Data are presented as the means \pm SEMs. $###p < 0.001$ by RM two-way ANOVA; $**p < 0.01$, $***p < 0.001$ by t test.

behavioral trajectories [23]. Notably, MoSeq does not pre-specify the number or identity of behavioral syllables; rather, it learns these features on a per-experiment basis. This flexible, detailed analysis proves especially valuable for detecting subtle deficits that might not be apparent through conventional behavioral assessments [39].

Traditional behavioral assessments often rely on aversive stimuli (such as bright light or electric shock) or rewarding stimuli (such as social interaction or food), which are specifically designed to focus

on particular aspects of animal behavior. However, such stimuli can induce anxiety in sensitive animals, such as Shank3 homozygous mice, as observed in this study. This anxiety can confound data interpretation. By employing MoSeq, we identified increased grooming and immobility in Shank3 homozygous mice. Additionally, these animals displayed less "upright" behavior, a posture in which the mouse rears up on its hind legs, a critical behavior for the development of allocentric spatial mapping [40]. Interestingly, we also observed changes in head movements:

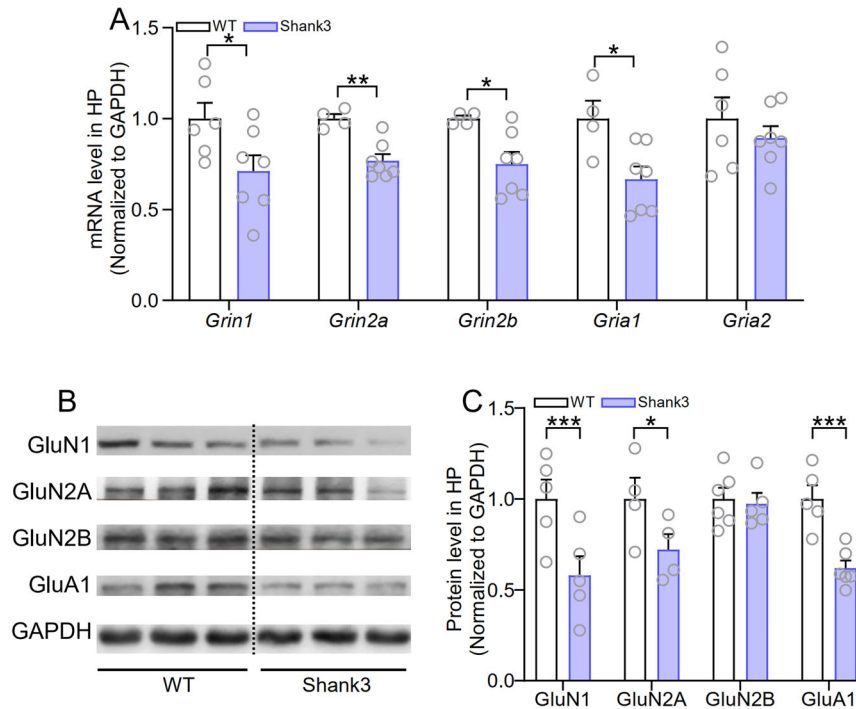


Fig. 6 Downregulation of hippocampal NMDA and AMPA subunits in Shank3 mice. **A** Bar graph of normalized mRNA levels of *Grin1*, *Grin2a*, *Grin2b*, *Gria1* and *Gria2* in WT and Shank3 mice ($n = 4-6$ mice in each group; *Grin1*: $p = 0.02$; *Grin2a*: $p = 0.0011$; *Grin2b*: $p = 0.0108$; *Gria1*: $p = 0.01$; *t* test). **B** Representative Western blot images. **C** Bar graph of normalized protein expression levels of GluN1, GluN2A, GluN2B, and GluA1 in the hippocampus of WT and Shank3 mice ($n = 4-6$ in each group; GluN1: $p = 0.012$; GluN2A: $p = 0.049$; GluA1: $p < 0.001$; *t* test). Data are presented as the means \pm SEMs. * $p < 0.05$, ** $p < 0.01$, *** $p < 0.001$ by *t* test. See also supplementary Fig. 3.

these animals exhibited less “head-down” behavior, but more “head-up” movements. While these fine motor changes are not directly linked to schizophrenia, they may offer novel behavioral features for further investigation. Additionally, correlations between fine behaviors and traditional behavioral assays were not calculated, as the data were generated from different batches rather than from the same batch, which represents a limitation of this study.

Behavioral characteristics of R1117X Shank3 mice and alternative behavioral paradigms

Shank3 mice exhibit notable abnormalities in various behavioral domains, including motor function, pain perception, sensory gating, and learning memory. Additionally, these mice display heightened anxiety-like behavior when exposed to novel environments. A detailed comparison of these findings is provided in Table 4, based on the previous study [17].

The severe anxiety observed in Shank3 homozygous mice—reported in both prior studies (e.g., decreased center vs. periphery time in the OFT, less time spent in the open arms of the EPM) [17] and in the current research (reduced movement in both the OFT and EPM)—suggests that behavioral assays involving aversive stimuli, such as the BM test (which uses bright light), may not be suitable for accurately evaluating cognition in these animals. Furthermore, Shank3 homozygous mice exhibit reduced pain sensitivity, making active/passive avoidance tests, which involve novel apparatus and foot shocks, unsuitable for assessing learning and memory. To address these challenges, we utilized the FED3 system [24], an automated, home-cage-based platform designed to monitor food self-administration, minimizing the effects of anxiety. The results revealed deficits in the ability of Shank3 homozygous mice to learn food self-administration, a behavior that involves several brain regions, including the ventral medial prefrontal cortex (mPFC) [41], olfactory areas, and the hippocampus [42]. Using the MWM, we also observed severe

impairments in hippocampus-dependent spatial learning and memory in these animals.

Collectively, these behavioral findings highlight several key characteristics of Shank3 homozygous mice: 1) abnormal sensory processing of pain and sound, along with PPI deficits; 2) severe anxiety and immobility in novel environments; and 3) significant learning and memory deficits. These traits position the Shank3 homozygous mouse as an ideal animal model for schizophrenia, encompassing positive, negative, and cognitive phenotypes. Additionally, these findings underscore the limitations of traditional behavioral assays, particularly for animals exhibiting high anxiety due to novel environments and aversive stimuli. Researchers must interpret behavioral data with caution, and consider incorporating newer home-cage-based tests like FED3 or machine learning-based 3D fine behavioral analysis methods, such as MoSeq, to enable more detailed behavioral characterization. Clinically, it is important to account for novel environment-induced anxiety during patient assessments, as this may lead to inaccurate results. Clinical diagnosis could benefit from incorporating behavioral assessments conducted in a familiar environment. Longitudinal monitoring of daily behavioral phenotypes, conducted in a familiar setting (e.g., the patient’s home), may provide a more accurate representation of their conditions.

Characteristics of Shank3-related hippocampal dysfunction

Previous studies have focused primarily on synaptic function within the cortex and striatum [17], reporting reductions in key synaptic proteins such as PSD93, SynGAP, NR1, NR2A, and NR2B in the striatum of adolescent Shank3-deficient mice, whereas basic synaptic transmission remains unaffected. In adult mice, significant synaptic deficits emerge in both the prefrontal cortex and striatum (both amplitude and frequency of miniature excitatory postsynaptic currents in medium spiny neurons (MSNs)). These deficits were accompanied by decreased NMDA currents in MSNs,

Table 4. Comparison of behavioral phenotypes in R1117X Shank3 mutant mice.

Behavioral tests	(Zhou et al., [17])		This study		Comments for Homo
	Het	Homo	Het	Homo	
Sensory	Pain: Von Frey test	\	\	Normal	Higher threshold
	Hearing: ABR	\	\	\	Reduced ABR threshold in respond to high frequency (16–32 kHz) stimulation. Impaired
Motor	Acoustic startle response	Normal	Impaired	\	Impaired
	PPI	Normal	Mild impaired	\	Increased PPI
	Rotarod	Normal	Impaired	Slightly impaired	Severely impaired
	Locomotor (OFT)	Slightly reduced	Reduced	Normal	Significantly reduced movement speed in novel environment (OFT), but normal in homecage.
Stereotyped behavior	Grooming	Normal	Slightly increased	Normal	Less grooming within 15 min but increased in a time window of 1 h.
	Marble burying	\	\	Less buried marbles.	Less buried marbles.
Anxiety	OFT	Decreased center vs periphery ratio.	Decreased center vs periphery ratio.	Reduced activity in the center area.	Reduced activity in the center area.
	EPM	Less time in open arms.	Less time in open arms.	Less entries in open arms.	Less entries and time in open arms.
Depression	TST & FST	\	\	Less immobility time.	Decreased latency to immobility.
	Three chambers	Impaired social preference and social novelty.	Impaired social preference and social novelty.	\	The increased social dominance may be due to immobility in novel tube.
Learning & memory	Social dominant (Tube test)	Increased	Increased	Increased	Increased
	T maze	\	Normal	\	\
Barnes Maze	\	\	\	Normal	Decreased movement and investigation time to both correct and incorrect holes (potential anxiety due to strong bright light stimulation).
	Active/passive avoidance	\	\	Increased latency to avoidance to avoidance.	Increased latency to avoidance (potential insensitive to electric shock).
MWM	\	\	\	\	Deficits in spatial learning and memory.
	FED3	\	\	\	Slower to learn self-administration of food reward at home cage.

ABR auditory brainstem response, EPM elevated plus maze, FED3 feeding experimentation device version 3, FST forced swimming test, Het heterozygous, Homo homozygous, MWM morris water maze, OFT open field test, PPI prepulse inhibition, TST tail suspension test, \ not performed. Tests with bold font indicate new experiments carried out specifically in this study.

as well as reductions in NR1 (both striatum and cortex) and NR2B (striatum only).

Extending this investigation to the hippocampus in this study, we observed similar dysfunctions in synaptic transmission, with suppressed input/output of fEPSPs. The PPR across various intervals was significantly lower in Shank3-deficient mice than in control mice, indicating deficits in short-term synaptic plasticity and presynaptic transmission. Further analysis of long-term synaptic potentiation revealed that the enhancement induced by TBS was notably weaker in Shank3-deficient mice, with effects dissipating within 30 min. These findings suggest that basic synaptic transmission, short-term facilitation, and both the induction and maintenance of LTP in the hippocampus are impaired in Shank3-deficient mice, which aligns with their observed learning and memory deficits.

Quantitative PCR and Western blot analysis of hippocampal tissue further revealed reduced transcription and expression levels of GluN1 and GluA1. These findings suggest that synaptic transmission in Shank3 homozygous mice is severely impaired in the cortex, striatum, and hippocampus, with brain region-specific molecular changes. The altered expression of glutamatergic receptors supports these electrophysiological findings, as AMPA receptors are critical for LTP induction and NMDA receptors play a key role in LTP maintenance. These deficits likely contribute to the observed learning and memory impairments in these animals.

Morphological analyses revealed a reduction in the density of dendritic spines in layer 3 pyramidal neurons of the prefrontal cortex, as confirmed by Golgi staining [17]. In parallel, Nissl staining from this study provided insight into neuronal development within the hippocampus, revealing significant thickening of the CA3 and DG regions, alongside an increase in neuron numbers. These morphological abnormalities in the hippocampus likely contribute to the cognitive deficits, particularly in learning and memory, observed in Shank3-deficient mice.

Behavioral and synaptic impact of different SHANK3 mutations

Mutations in *SHANK* genes (*SHANK1*, *SHANK2*, *SHANK3*) are well known to produce pronounced behavioral alterations in mice, mirroring aspects of neuropsychiatric disorders. SHANK proteins, often referred to as master scaffolds, are crucial for synapse development and function because of their role in organizing excitatory synapses [43]. Mutations in *SHANK3*, in particular, are strongly linked to ASD and PMDS, making *SHANK3* mutations a high-risk genetic cause of autism. Previous studies have faced challenges in targeting *SHANK3* isoforms in mouse models, likely because of the gene's multiple promoters [44].

One mutation, InsG3728 [16], which results from a single guanine insertion in exon 21 of *Shank3*, causes a frameshift and premature stop codon. This leads to the loss of a critical high-molecular-weight isoform of Shank3 at the synapse. Mice harboring this mutation display a range of deficits, including impaired spatial learning, motor coordination, and sensory processing, as well as disrupted hippocampal synaptic transmission and plasticity, particularly affecting NMDA receptor-mediated responses.

A similar mutation, InsG3680 [17], which is also associated with an autism-linked insertion in exon 21, produces distinct behavioral and synaptic abnormalities. Mice with this mutation show increased repetitive grooming, anxiety-like behaviors, and social interaction deficits, along with early synaptic transmission impairments in the striatum.

Furthermore, *Shank3* C-terminal deletions [13], which remove the Homer and Cortactin binding domains, result in autism-like behaviors and severely diminished NMDA receptor function in the prefrontal cortex. This mutation also leads to actin filament loss and disruptions in Rac1/PAK activity, which is essential for synaptic integrity. Increased activity of cofilin, the main actin

depolymerizing factor, exacerbates these cytoskeletal abnormalities, further contributing to synaptic deficits.

In contrast, the R1117X mutation in *Shank3*, while showing some overlap with ASD phenotypes such as grooming and anxiety-like behaviors, results in more pronounced learning and memory impairments. Synaptic defects in the prefrontal cortex, which are observed in both mutant mice and schizophrenia patients [17], suggest a broader role for *Shank3* mutations beyond autism. The elevated calcium transients in the dendritic spines of R1117X mutants point to a loss of inhibitory control, which is mediated by reduced NMDAR currents and impaired firing of somatostatin-expressing interneurons. This disruption in dendritic inhibition may underlie key aspects of *Shank3* dysfunction [45].

Notably, R1117X *Shank3* mice display deficits in LTP in the hippocampus, which is a core indicator of learning and memory processes. The reduced fEPSPs responses to TBS stimulation are similar to those observed in other ID models [46]. Given the importance of NMDARs and AMPARs in cognitive function [47], the reduced expression of GluN1 and GluA1 observed in these mice likely contributes to their impaired intellectual abilities, reinforcing the critical role of glutamatergic signaling in *Shank3*-related neurodevelopmental disorders.

Taken together, our results demonstrate that homozygous R1117X mutant *Shank3* mice represent a valuable model for schizophrenia associated with severe ID. These mice exhibit altered hippocampal morphology, impaired synaptic transmission, downregulation of NMDA receptor-related mRNA and protein expression, accompanied by severe deficits in learning and memory. These findings suggest that the R1117X mutant *Shank3* mouse model could be an important tool for future research into schizophrenia-related neurodevelopmental disorders. Additionally, our study emphasizes the necessity of using a comprehensive set of behavioral screening tests when evaluating schizophrenia models, particularly those involving home-cage assessments. This approach would provide a more accurate portrayal of behavioral patterns and enhance the reliability of the results. From a clinical perspective, our findings support the incorporation of daily behaviors into the diagnostic process for schizophrenia. Moreover, prior to clinic assessments, it is advisable to first alleviate the patient's anxiety. For individuals experiencing severe anxiety, returning them to a familiar environment before conducting further evaluations may help ensure a more accurate diagnosis.

DATA AVAILABILITY

The datasets used and/or analyzed during the current study are available from the corresponding author upon reasonable request.

REFERENCES

- Silverman JL, Yang M, Lord C, Crawley JN. Behavioural phenotyping assays for mouse models of autism. *Nat Rev Neurosci*. 2010;11:490–502.
- De Rubeis S, He X, Goldberg AP, Poultnery CS, Samocha K, Cicek AE, et al. Synaptic, transcriptional and chromatin genes disrupted in autism. *Nature*. 2014;515:209–15.
- Qin L, Ma K, Wang ZJ, Hu Z, Matas E, Wei J, et al. Social deficits in Shank3-deficient mouse models of autism are rescued by histone deacetylase (HDAC) inhibition. *Nat Neurosci*. 2018;21:564–75.
- Zhang Q, Xing M, Bao Z, Xu L, Bai Y, Chen W, et al. Contactin-associated protein-like 2 (CNTNAP2) mutations impair the essential alpha-secretase cleavages, leading to autism-like phenotypes. *Signal Transduct Target Ther*. 2024;9:51.
- Weissberg O, Elliott E. The mechanisms of CHD8 in neurodevelopment and autism spectrum disorders. *Genes*. 2021;12:1133.
- Rein B, Yan Z. 16p11.2 copy number variations and neurodevelopmental disorders. *Trends Neurosci*. 2020;43:886–901.
- Leblond CS, Nava C, Polge A, Gauthier J, Huguet G, Lumbroso S, et al. Meta-analysis of SHANK mutations in autism spectrum disorders: a gradient of severity in cognitive impairments. *PLoS Genet*. 2014;10:e1004580.
- Uchino S, Waga C. SHANK3 as an autism spectrum disorder-associated gene. *Brain Dev*. 2013;35:106–10.
- Sheng M, Kim E. The shank family of scaffold proteins. *J Cell Sci*. 2000;113:1851–6.

10. Grabrucker AM, Schmeisser MJ, Schoen M, Boeckers TM. Postsynaptic ProSAP/Shank scaffolds in the cross-hair of synaptopathies. *Trends Cell Biol.* 2011;21:594–603.
11. Phelan K, McDermid HE. The 22q13.3 deletion syndrome (Phelan-McDermid syndrome). *Mol Syndromol.* 2011;2:186–201.
12. Betancur C, Buxbaum JD. SHANK3 haploinsufficiency: a “common” but under-diagnosed highly penetrant monogenic cause of autism spectrum disorders. *Mol Autism.* 2013;4:17.
13. Duffney LJ, Zhong P, Wei J, Matas E, Cheng J, Qin L, et al. Autism-like deficits in Shank3-deficient mice are rescued by targeting actin regulators. *Cell Rep.* 2015;11:1400–13.
14. Durand CM, Betancur C, Boeckers TM, Bockmann J, Chaste P, Fauchereau F, et al. Mutations in the gene encoding the synaptic scaffolding protein SHANK3 are associated with autism spectrum disorders. *Nat Genet.* 2007;39:25–7.
15. Dellling JP, Boeckers TM. Comparison of SHANK3 deficiency in animal models: phenotypes, treatment strategies, and translational implications. *J Neurodev Disord.* 2021;13:55.
16. Speed HE, Kouser M, Xuan Z, Reimers JM, Ochoa CF, Gupta N, et al. Autism-associated insertion mutation (InsG) of Shank3 exon 21 causes impaired synaptic transmission and behavioral deficits. *J Neurosci.* 2015;35:9648–65.
17. Zhou Y, Kaiser T, Monteiro P, Zhang X, Van der Goes MS, Wang D, et al. Mice with Shank3 mutations associated with ASD and schizophrenia display both shared and distinct defects. *Neuron.* 2016;89:147–62.
18. Gauthier J, Champagne N, Lafreniere RG, Xiong L, Spiegelman D, Brustein E, et al. De novo mutations in the gene encoding the synaptic scaffolding protein SHANK3 in patients ascertained for schizophrenia. *Proc Natl Acad Sci USA.* 2010;107:7863–8.
19. Rapanelli M, Tan T, Wang W, Wang X, Wang ZJ, Zhong P, et al. Behavioral, circuitry, and molecular aberrations by region-specific deficiency of the high-risk autism gene Cul3. *Mol Psychiatry.* 2021;26:1491–504.
20. Modi AD, Parekh A, Pancholi YN. Evaluating pain behaviours: widely used mechanical and thermal methods in rodents. *Behav Brain Res.* 2023;446:114417.
21. Tan T, Wang W, Williams J, Ma K, Cao Q, Yan Z. Stress exposure in dopamine D4 receptor knockout mice induces schizophrenia-like behaviors via disruption of GABAergic transmission. *Schizophr Bull.* 2019;45:1012–23.
22. Lin S, Gillis WF, Weinreb C, Zeine A, Jones SC, Robinson EM, et al. Characterizing the structure of mouse behavior using motion sequencing. *Nat Protoc.* 2024;19:3242–91.
23. Wiltshchko AB, Tsukahara T, Zeine A, Anyoha R, Gillis WF, Markowitz JE, et al. Revealing the structure of pharmacobehavioral space through motion sequencing. *Nat Neurosci.* 2020;23:1433–43.
24. Nguyen KP, O’Neal TJ, Bolonduro OA, White E, Kravitz AV. Feeding experimentation device (FED): a flexible open-source device for measuring feeding behavior. *J Neurosci Methods.* 2016;267:108–14.
25. Huang Z, Tan T, Du Y, Chen L, Fu M, Yu Y, et al. Low-frequency repetitive transcranial magnetic stimulation ameliorates cognitive function and synaptic plasticity in APP23/PS45 mouse model of Alzheimer’s disease. *Front Aging Neurosci.* 2017;9:292.
26. Zhou C, Yan S, Qian S, Wang Z, Shi Z, Xiong Y, et al. Atypical response properties of the auditory cortex of awake MECP2-overexpressing mice. *Front Neurosci.* 2019;13:439.
27. Li ZW, Tang H, Chen XX, Li XX, Xu HH, Chen MH, et al. Urolithin B attenuates cerebral ischemia-reperfusion injury by modulating Nrf2-regulated anti-oxidation in rats. *Neuroscience.* 2024;538:46–58.
28. Dordoe C, Wang X, Lin P, Wang Z, Hu J, Wang D, et al. Non-mitogenic fibroblast growth factor 1 protects against ischemic stroke by regulating microglia/macrophage polarization through Nrf2 and NF-kappaB pathways. *Neuropharmacology.* 2022;212:109064.
29. Wang D, Liu F, Zhu L, Lin P, Han F, Wang X, et al. FGF21 alleviates neuroinflammation following ischemic stroke by modulating the temporal and spatial dynamics of microglia/macrophages. *J Neuroinflammation.* 2020;17:257.
30. Wang W, Tan T, Yu Y, Huang Z, Du Y, Han H, et al. Inhibition of AMPAR endocytosis alleviates pentobarbital-induced spatial memory deficits and synaptic depression. *Behav Brain Res.* 2018;339:66–72.
31. Miller EA, Kastner DB, Grzybowski MN, Dwinell MR, Geurts AM, Frank LM. Robust and replicable measurement for prepulse inhibition of the acoustic startle response. *Mol Psychiatry.* 2021;26:1909–27.
32. Zeng L, Zhou W, Bing D, Xie L, Wang X, Zhang G. Protocol for assessing auditory brainstem response in mice using a four-channel recording system. *STAR Protoc.* 2022;3:101251.
33. Cording KR, Bateup HS. Altered motor learning and coordination in mouse models of autism spectrum disorder. *Front Cell Neurosci.* 2023;17:1270489.
34. Drapeau E, Riad M, Kajiwara Y, Buxbaum JDJE. Behavioral phenotyping of an improved mouse model of Phelan–McDermid syndrome with a complete deletion of the Shank3 gene. *eNeuro.* 2018;5:ENEURO.0046-18.2018.
35. Ball TM, Gunaydin LA. Measuring maladaptive avoidance: from animal models to clinical anxiety. *Neuropsychopharmacology.* 2022;47:978–86.
36. Jeffery KJ. The hippocampus: from memory, to map, to memory map. *Trends Neurosci.* 2018;41:64–66.
37. Woelfle S, Pedro MT, Wagner J, Schon M, Boeckers TM. Expression profiles of the autism-related SHANK proteins in the human brain. *BMC Biol.* 2023;21:254.
38. Yang X, Gong R, Qin L, Bao Y, Fu Y, Gao S, et al. Trafficking of NMDA receptors is essential for hippocampal synaptic plasticity and memory consolidation. *Cell Rep.* 2022;40:111217.
39. Fatima G, Ashiqquzaman A, Kim SS, Kim YR, Kwon H-S, Chung E. Vascular and glymphatic dysfunction as drivers of cognitive impairment in Alzheimer’s disease: insights from computational approaches. *Neurobiol Dis.* 2025;208:106877.
40. Shan X, Contreras MP, Sawangjit A, Dimitrov S, Born J, Inostroza M. Rearing is critical for forming spatial representations in pre-weanling rats. *Behav Brain Res.* 2023;452:114545.
41. Warren BL, Mendoza MP, Cruz FC, Leao RM, Caprioli D, Rubio FJ, et al. Distinct fos-expressing neuronal ensembles in the ventromedial prefrontal cortex mediate food reward and extinction memories. *J Neurosci.* 2016;36:6691–703.
42. Madangopal R, Szelenyi ER, Nguyen J, Brenner MB, Drake OR, Pham DQ, et al. Incubation of palatable food craving is associated with brain-wide neuronal activation in mice. *Proc Natl Acad Sci USA.* 2022;119:e2209382119.
43. Monteiro P, Feng G. SHANK proteins: roles at the synapse and in autism spectrum disorder. *Nat Rev Neurosci.* 2017;18:147–57.
44. Zhu L, Wang X, Li XL, Towers A, Cao X, Wang P, et al. Epigenetic dysregulation of SHANK3 in brain tissues from individuals with autism spectrum disorders. *Hum Mol Genet.* 2014;23:1563–78.
45. Ali F, Shao L-X, Gerhard DM, Sweasy K, Pothula S, Pittenger C, et al. Inhibitory regulation of calcium transients in prefrontal dendritic spines is compromised by a nonsense Shank3 mutation. *Mol Psychiatry.* 2021;26:1945–66.
46. Bavley CC, Rice RC, Fischer DK, Fakira AK, Byrne M, Kosovsky M, et al. Rescue of learning and memory deficits in the human nonsyndromic intellectual disability cereblon knock-out mouse model by targeting the AMP-activated protein kinase-mTORC1 translational pathway. *J Neurosci.* 2018;38:2780–95.
47. Venkatesan S, Binko MA, Mielnik CA, Ramsey AJ, Lambe EK. Deficits in integrative NMDA receptors caused by Grin1 disruption can be rescued in adulthood. *Neuropsychopharmacology.* 2023;48:1742–51.

AUTHOR CONTRIBUTIONS

JG and SW conducted behavioral and electrophysiological experiments, performed histology, analyzed the data, and wrote the manuscript draft. JY (Jie Yang), TY, WS, XC, and LH contributed to part of behavioral tests and histology. JY (Jingxuan Yang) and JL analyzed the Moseq data. PL, TY and WW performed the molecular and part of behavioral experiments, and analyzed the data. RP and YZ carried out the ABR testing. JG, SW, and TT designed the experiments. TT supervised the project and revised the manuscript.

FUNDING

This study was funded by the National Natural Science Foundation of China (82471536); Wenzhou Science and Technology Projects (ZY2023006, 2024R2002); and Oujiang Laboratory (OJQD2022002) to T.T.

COMPETING INTERESTS

The authors declare no competing interests.

ETHICS APPROVAL

The animal study was reviewed and approved by the Experimental Animal Ethics Review Committee of Oujiang Laboratory. All methods were performed in accordance with the Guide for the Care and Use of Laboratory Animals and relevant regulations.

ADDITIONAL INFORMATION

Supplementary information The online version contains supplementary material available at <https://doi.org/10.1038/s41398-025-03505-1>.

Correspondence and requests for materials should be addressed to Tao Tan.

Reprints and permission information is available at <http://www.nature.com/reprints>

Publisher’s note Springer Nature remains neutral with regard to jurisdictional claims in published maps and institutional affiliations.



Open Access This article is licensed under a Creative Commons Attribution-NonCommercial-NoDerivatives 4.0 International License, which permits any non-commercial use, sharing, distribution and reproduction in any medium or format, as long as you give appropriate credit to the original author(s) and the source, provide a link to the Creative Commons licence, and indicate if you modified the licensed material. You do not have permission under this licence to share adapted material derived from this article or parts of it. The images or other third party material in this article are included in the article's Creative Commons licence, unless indicated otherwise in a credit line to the material. If material is not included in the article's Creative Commons licence and your intended use is not permitted by statutory regulation or exceeds the permitted use, you will need to obtain permission directly from the copyright holder. To view a copy of this licence, visit <http://creativecommons.org/licenses/by-nc-nd/4.0/>.

© The Author(s) 2025